Performance analysis of interlinking converter exchanging power between AC/DC renewable microgrids with advanced control technique

Mamatha Seeramshetti, Mallesham Gaddam
Department of Electrical Engineering, University College of Engineering, Osmania University, Hyderabad, India

| Article Info	ABSTRACT
	In a distribution system there are many types of AC/DC microgrids integrated at different locations. These microgrids may contain conventional or renewable sources which generate power using natural resources. The power generated by these microgrid sources is uncertain as the natural resources are unpredictable. Therefore, powers from these AC/DC micro grids need to be shared so as to compensate the load demand throughout the distribution system. An interlinking converter (ILC) is connected between the AC/DC microgrids operated by a novel advanced PQ control technique. Both the DC and AC microgrids are interconnected through ILC achieving power exchange between them as per the power demand and generation on both microgrids. Different operating conditions are considered for the analysis and the simulation of these modules are done using MALTAB/Simulink software. Several parameters like DC link voltage, ILC currents, point of common coupling (PCC) frequency, total harmonic distortions (THDs) and active power values are considered for validating the stability of the considered system. *This is an open access article under the CC BY-SA license.*
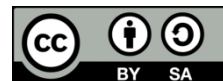
Corresponding Author:

Mamatha Seeramshetti
Department of Electrical Engineering, University College of Engineering, Osmania University
Hyderabad, India
Email: mamata.seeramshetti@gmail.com

1. INTRODUCTION

Energy generation through conventional methods have created global warming resulting in climatic disasters and creating dilapidated conditions for the living beings. It has become obligatory for us to generate power using natural resources like solar irradiation, wind, bio-gas, and tidal or hydro. These renewable sources are named as distribution generators (DGs) which are connected on the distribution side of the grid system [1]. Integration of these DG units makes it a smart grid as the power generation is controlled by a central control module. In some cases when the conventional main grid is completely isolated or unavailable specifically in remote areas, the smart grid has to be a standalone system.

The standalone smart grid with multiple renewable sources and energy storage units (ESU) forms a microgrid (MG). The inclusion of ESUs is mandatory as the system is operating in standalone condition. The unpredictable fluctuating renewable power generation may damage the load without the ESUs [2]. The MG is a miniature grid with lower rating modules connected at a point of common coupling (PCC) exchanging power. Considerably there are two types of MGs: i) AC MG and ii) DC MG which are named as per the structure of the system. The AC MG comprises of an alternating current (AC) point of common coupling (PCC), where multiple sources are connected through 3-ph AC lines & the DC MG is designed with common DC link where all the modules are connected [3].

The structural differences restrict the AC MG and DC MG exchange power as per the load demand on either of the MG [4]. Therefore, to make the system reliable and robust to achieve full compensation of load demand on either of the MGs an interlinking converter (ILC) is connected between the MGs [5]. The ILC is a 3-ph voltage source converter (VSC) comprising of 6- insulated-gate bipolar transistor (IGBT) switches operated by a normalized droop control method. The ILC has a DC side with two terminals and an AC side with three terminals interconnected between the DC and AC MGs [6]. The proposed structure with multiple renewable sources and energy storage units on AC and DC MGs connected through an ILC can be observed in Figure 1.

As per Figure 1 the DC MG comprises of photovoltaic (PV) source, wind farm, battery storage module and AC MG comprises of fuel cell plant, wind farm, super capacitor (SC) storage module. All the renewable sources are connected to DC or AC bus through individual unidirectional converters [7]. However, the storage modules battery and SC are connected through individual bidirectional converters for exchange of power. The PV source is a solar plant where multiple solar panels are connected in series and parallel combinations generating power using solar irradiation. As the solar power generation is done at unregulated DC voltage magnitudes a DC-DC boost converter is adopted to stabilize the voltage and extract maximum power from PV panels. The DC-DC boost converter switch is controlled by perturb and observe (P&O) maximum power point tracking (MPPT) algorithm with feedback from PV source voltage and current. Similar to the PV source the wind farm source has a wind turbine coupled to permanent magnet synchronous generator (PMSG) connected to a unidirectional buck-boost converter controlled by power signal feedback (PSF) MPPT. The boost converter of the fuel cell plant, battery module, and SC module is controlled by 'constant voltage' controller with voltage reference. Each source is operated by their own individual controller extracting maximum power and exchange power of the sources [8]. These two MGs AC bus and DC bus are connected through a single or multiple ILC units exchanging power between them.

The complete design and methodologies of the devices and modules connected in the proposed hybrid MG system is discussed in further sections of the paper: i) Section 1, the introduction to the proposed topology and devices integrated is presented; ii) Internal design circuit of each renewable and storage module is discussed in section 2; iii) Section 3 comprises of modeling of ILC module with control structure design of the ILC; iv) The simulation of the presented hybrid MG system with ILC is carried out using MATLAB/Simulink support generating graphs shown in section 4; and v) The performance of the proposed system is validated by the graphs generated in the simulation using different operating conditions and conclusion to the paper is included in section 5.
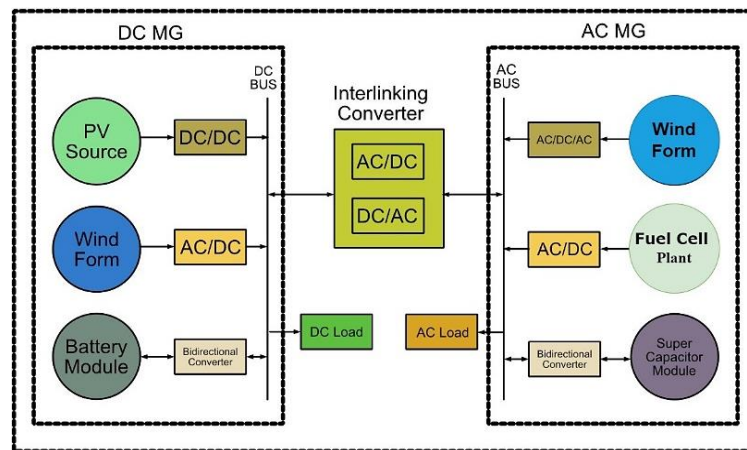

Figure 1. Proposed hybrid microgrid structure with ILCs

2. HYBRID MG CONFIGURATION

As previously mentioned in section 1, the hybrid MG is a combination of AC MG and DC MG interconnected through a single or multiple ILC modules. The AC MG has individual inverters connected to each source for sharing power at AC bus [9]. The DC MG has only the DC-DC converters, exchanging power at DC bus. Different choice of renewable sources on both MGs are selected to create versatility of the system [10]. The DC MG comprises of a PV source with PV panels connected to boost converter operated by a MPPT control [11]. Along with PV source a wind farm is also integrated with PMSG wind turbine connected diode bridge rectifier and buck-boost (BB) converter. For energy storage and support, a battery backup module is connected through bidirectional DC-DC converter (BDC) [12].

On the AC MG a fuel cell plant is considered with boost converter operated by constant voltage (CV) control connected to 3-ph VSC. The same structure of wind farm in DC MG is used in AC MG but with added 3-ph VSC connected to BB converter [13]. And for the energy storage, a SC module is connected through BDC with 3-ph VSC. The both MGs are interconnected with a 6-swith IGBT VSC circuit topology named as ILC. The complete structure of the proposed system with circuit configuration can be observed in Figure 2.

Each module in the given hybrid MG has its own circuit topology operated with individual controllers. On the DC MG side, the PV source boost converter is operated by traditional incremental conductance MPPT technique with feedback signals of PV voltage and current. The duty ratio of the switch is varied as per the change in PV voltage, current, and relational conditions given in the MPPT control. The PMSG wind farm is a 3-ph AC renewable source which generates power from wind natural source. The dynamic braking resistors (DBR) is connected to the PMSG for conversion of variable AC (as wind speeds are unpredictable) to variable DC. For DC voltage stability and maximum power extraction from PMSG, a BB converter is connected to the DBR operated by power signal feedback (PSF) MPPT [14].

The battery is connected to a BDC operated by voltage feedback controller which takes voltage feedback from the DC bus. A proportional Integral or PI controller is integrated for generation of duty ratio to the complementary switches of the BDC. All the positive and negative terminals of the DC-DC converters are coupled forming a DC bus. On the AC MG side the fuel cell is connected to boost converter operated by CV control and a 3-ph inverter is connected for conversion of DC-AC voltages. The wind farm is similar to the DC MG wind farm with only added 3-ph inverter. The storage module is SC connected BDC operated by voltage feedback controller. A 3-ph bidirectional VSC is connected to the SC unit [15].

All the 3-ph inverters of the AC MG system are connected with common terminals forming an AC bus. These inverters of the renewable sources and SC unit are operated by synchronous reference frame (SRF) controller [16]. The SRF control ensures synchronization of AC voltage of each module to avoid unnecessary harmonics in the system. The SRF ensures there is a synchronized exchange of power between the modules [17]. The AC MG and DC MG are interconnected by an ILC operated using 'normalized droop control method' which is discussed in further section. The ILC exchanges power between the MGs compensating the power demand on either of the MGs as per the requirement.
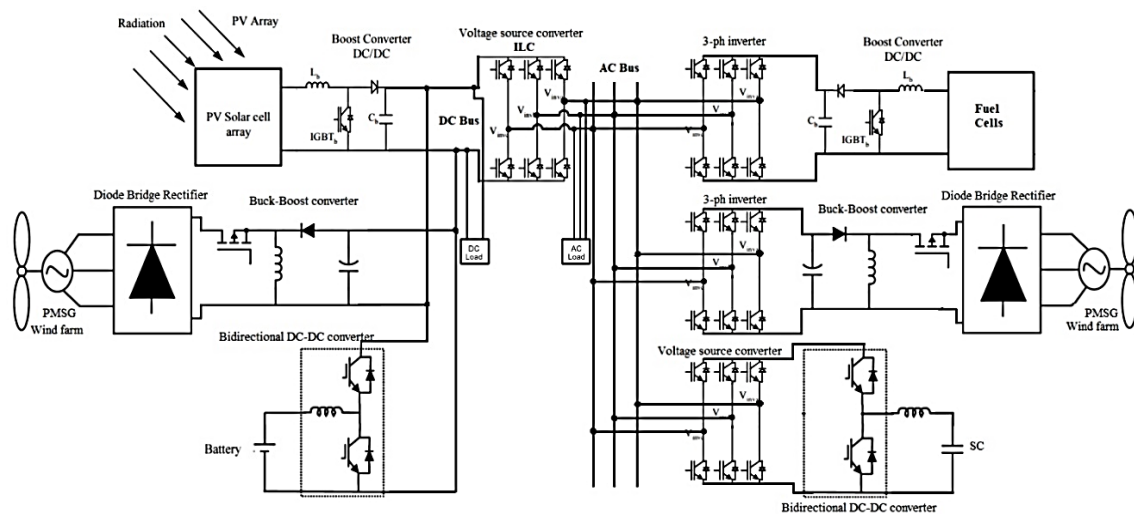

Figure 2. Circuit configuration of proposed hybrid MG

3. CONTROL DESIGN

The ILC in the hybrid MG is controlled by sine-pulse width modulation (PWM) technique, which generates pulses for the IGBT switches [18]. The 6-switch ILC (VSC) presented in Figure 2 needs to be controlled by a feedback controller for exchange of power between the MGs. The conventional controller is SRF method which has the capability to maintain the DC link voltage and synchronize the VSC to the AC MG voltages. The conventional SRF controller design is presented in Figure 3.

As observed in Figure 3 the reference voltage signals are generated by feedback signals from the grid voltages (Va, Vb, Vc) and inverter currents (Ia, Ib, Ic). The complex signals are reduced to simple integer format using Park's transformations for arithmetic calculations. The below are the reference signal $(V \mid \mid d\, V_q)$ equations generated by the SRF controller design for controlling the ILC, as in (1)-(4).

$$V_d = Ud + Vd + L\omega I_q \tag{1}$$

$$V_q = Uq + Vq - L\omega I_d \tag{2}$$

$$U_d = (i_d - i_d)\left(k_p + \frac{k_i}{s}\right) \tag{3}$$

$$U_q = (i_q - i_q)\left(k_p + \frac{k_i}{s}\right) \tag{4}$$

Here, V_d, V_q are the dq grid voltages, I_d, I_q are the dq inverter currents, i_d, i_q are the dq current references, L is the filter inductance, ω is the angular frequency of the grid voltages, k_p, k_i are the proportional and integral gains of the current controller. For no exchange of reactive power i_q is taken as zero and the i_d is expressed as (5).

$$i_d = (V_{dc} - V_{dc})\left(k_{pv} + \frac{k_{iv}}{s}\right) \tag{5}$$

Here, V_{dc} and V_{dc} are the reference and measured DC link voltages on the DC side of the ILC. The k_{pv}, k_{iv} are the proportional and integral gain of voltage controller [19]. Due to no power feedback signals the SRF controller can only transfer power from DC side to the AC side of the hybrid MG. This conventional controller has no capability to make the ILC deliver power to the DC side of the system. Hence, an advanced control structure is needed which can operate the ILC in both directions.

The reference sin signals are generated by 'normalized droop control method' with feedback from DC bus voltage (V_{dc}) and AC bus voltages (V_{abc}). The active and reactive power exchange between AC MG and DC MG is controlled by direction of current reference generated. The complete structure of 'normalized droop control method' can be seen in Figure 4. In order to generate normalized values of $V_{dc\,PU}$ and f_{PU} from Vdc and V_{abc}, the following expressions are considered, as in (6) and (7).

$$V_{dcPu} = \frac{(V_{dcmax} + V_{dcmin}) * (V_{dc} - 0.5)}{(V_{dcmax} - V_{dcmin}) * 0.5} \tag{6}$$

$$f_{Pu} = \frac{(f_{max} + f_{min}) * (f - 0.5)}{(f_{max} - f_{min}) * 0.5} \tag{7}$$

Here, $V_{dc,max}$ is maximum DC voltage (1.1 * $V_{dc\,ref}$), $V_{dc,min}$ is minimum DC voltage (0.9 * $V_{dc,ref}$), $V_{dc,ref}$ is the reference DC Bus voltage (set as per system configuration), V_{dc} is the measured DC bus voltage. f_{max} is maximum frequency (+5% of fundamental system frequency), f_{min} is the minimum frequency (-5% of fundamental system frequency) and 'f' is measured AC bus frequency [20]. The PU (per unit) (1) and (2) are compared generating error signal 'e' passed through active power constant Kp generating reference active power (P*) expressed as (8).
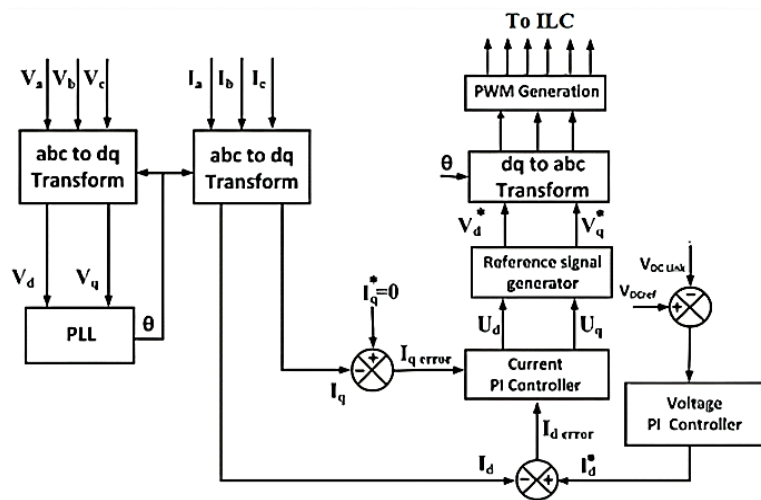
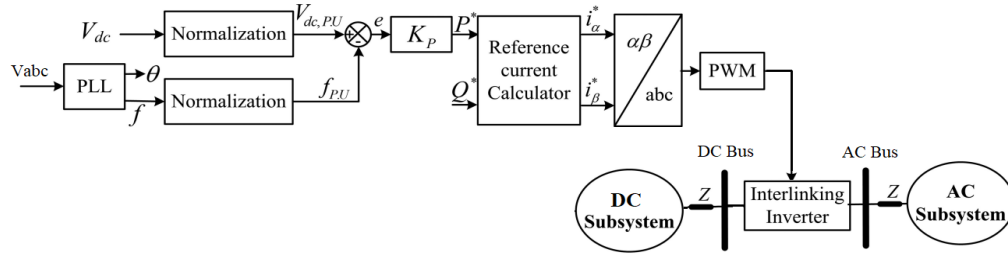$$P = K_p * (V_{dcPU} - f_{PU}) \tag{8}$$

Figure 3. SRF controller

Figure 4. Normalized droop control method structure

The reactive power reference Q* can be considered to be any finite value (+ve or -ve) or zero for no reactive power exchange [21]. From the reference active and reactive powers (P* and Q*) the final reference current components (I_α, I_β regenerated by (9) and (10).

$$I_\alpha = P \tag{9}$$

$$I_\beta = P \tag{10}$$

Here, k_1 and k_2 are the sensitivity constants for positive and negative sequences changed as per the response of the controller. are the positive and negative sequence voltage magnitudes of V_{abc} [22], [23]. V_α^+, V_α^-, V_β^+ and V_β^- are the positive and negative sequence $\alpha\beta$ voltages calculated using Clark's transformation expressed as (11) and (12).

$$V_\alpha = \frac{2}{3}V_a - \frac{1}{3}V_b - \frac{1}{3}V_c \tag{11}$$

$$V_\beta = \frac{1}{\sqrt{3}}V_b - \frac{1}{\sqrt{3}}V_c \tag{12}$$

The reference signals $I_\alpha \wedge I_\beta$ converted to sine signals to generate PWM pulses for the ILC using inverse Clark's transformation given as (13)-(15).

$$I_a = I_\alpha \tag{13}$$

$$I_b = \frac{-1}{2}I_\alpha + \frac{\sqrt{3}}{2}I_\beta \tag{14}$$

$$I_c = \frac{-1}{2}I_\alpha - \frac{\sqrt{3}}{2}I_\beta \tag{15}$$

The magnitude of the reference signals (I_{abc}) is adjusted by a gain, value set as per the sine PWM requirement for generation of pulses to the ILC IGBT switches [24]. The complete control modules are integrated into ILC and the simulation of the given system Figure 2 is modeled in the next section 4 [25].

4. RESULT ANALYSIS

Modeling and analysis of the given hybrid MG with multiple renewable sources, energy storage modules, loads, and ILC is carried out in MATLAB Simulink 9.3 software. For the modeling of sources and circuit topologies, blocks from 'Powersystem' toolbox in the Simulink library are considered. Each module is defined with specific parametric ratings for the simulation of the hybrid MG operating in different conditions. Table 1 are the system parameters considered for the hybrid MG modules configuration.

As per the given parameters, the simulation is run with different load demands on the AC MG and DC MG with variable natural resources. Different case load variations are considered and the simulations are validated. For the given cases different parameters are measured to analyze the stability of the system and the performance of ILC.

4.1. Case 1: step change of DC and AC loads

In the initial case 1 the renewable sources are operated in optimal condition with solar irradiation at 1000W/mt^2 and wind speed at 12 m/s. During these states, the PV source and wind farm generate maximum power which can be either utilized by the load or stored in battery and SC. As observed the DC MG has higher

renewable power generation as compared to AC MG. Different loads are connected on the DC side and AC side, with step change at a specific time. The complete simulation time taken is 1.5 sec, with a change in DC load at 0.5 sec and a change in AC load at 1sec. The step change in the loads is done by circuit breakers tripping ON at the mentioned times. Initially, the DC load is 20 kW which is step changed to 40 kW at 0.5 sec, later at 1 sec the AC load is changed to 20 kW which was 10 kW initially. The voltage and power graphs of all the modules as per the changes in the system are recorded and plotted with respect to time are given in Figure 5.

Figure 5 is the graph of modules powers on the DC MG generating 22 kW of solar power, 20 kW of wind power. The battery power changes from negative to positive representing charging and discharging conditions respectively. The battery stores power initially from 0-0.5 sec at 20 kW which is excess power generated by the PV source and wind farm. The battery power changes to positive as the load increases at 0.5 and 1 sec.

Table 1. System configuration parameters

| Name of the parameter	Values
PV source	V_{mp} = 54.7 V, I_{mp} = 5.58 A, V_{oc} = 64.2 V, I_{sc} = 5.96 A, N_s = 10, N_p = 10, P_{pv} = 30.5 kW
	L_b=1 mH, C_{in}=100 uF, MPPT = incremental conductance, dint = 0.5, f_s=5 KHz.
Wind farm DC MG	P_n = 35 kW, T_m = 125 Nm, V_{dc} = 560 V, N = 3000 rpm, R_s = 0.05Ω, L_s = 0.635 mH, φ = 0.192 V.s, p = 4, J = 0.011 kg.m^2.
	L_{bb} = 100uH, C_{in} = 1000 uF, MPPT = power signal feedback.
Wind farm AC MG	P_n = 6 kW, T_m = 41.4 Nm, V_{dc} = 300 V, N = 2300 rpm, R_s = 0.0918 Ω, L_s = 0.975 mH, φ = 0.1688 V.s, p = 4, J = 0.003945 kg.m^2.
	L_{bb} = 100 uH, C_{in} = 1000 uF, MPPT = power signal feedback.
Battery module	V_{bat} = 500 V, Capacity = 200 Ah, SOC_{int} = 90%
	L_{bdc} = 161 uH, C_{out} = 220 uF. K_p = 0.05, K_i = 0.0023, V_{dcref} = 750 V, f_s = 5 kHz.
Fuel cell plant	PEM-FC - V_{nom} = 400 V, I_{nom} = 50 A, V_{end} = 250V, I_{end} = 150 A. L_b = 1 mH, C_{in} = 100 uF, C_{out} = 1200 uF, V_{dcref} = 750 V, K_p = 0.05, K_i = 0.0023, f_s = 5 kHz, m = 0.89, L_f = 0.5 mH, C_f = 550 uF.
SC module	C_{dc} = 10 F, R_c = 8.9 mΩ, V_{rated} = 500 V, N_p = N_s = 1, V_{int} = 500 V, T = 25 °C. L_{bdc} = 161 uH, C_{out}=220uF.
	K_p = 0.05, K_i = 0.0023, V_{dcref} = 750 V, f_s = 5 kHz, m = 0.89, L_f = 0.5 mH, C_f = 550 uF.
ILC	R_{igbt} = 0.01 Ω, L_f = 0.5 mH, C_f = 550 uF, V_{dcref} = 750 V, K_p = 10, k_1 = k_2 = 1.
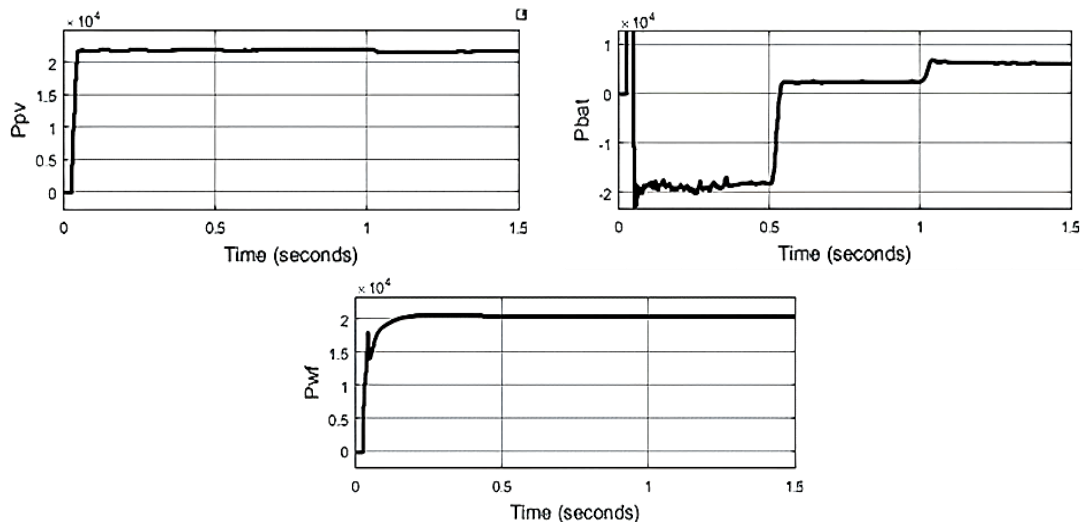
Figure 5. DC MG power of PV source, battery module, and wind farm on DC MG for case 1

Figure 6 is the DC link voltage measured at 750 V which is the reference voltage set in the voltage controller of the battery module. The DC load power demand can be observed in Figure 6 which step changes from 20 to 40 kW at 0.5 sec. The complete power delivered from the DC MG is plotted in Figure 7 which changes from 23 kW, 44 kW, and 47 kW at 0-0.5, 0.5-1, and 1-1.5 sec respectively. The value of the DC MG power delivery changes as per the load demand on the DC MG or AC MG. In Figure 7 it is observed that as per the changes in the load demand power, the power delivered by the ILC also changes from 3 to 6 kW at 1 sec as the AC MG load demand increases at 1 sec.

In Figure 8, the powers of all the AC MG modules are shown for case 1. The fuel cell plant power changes from 2 to 5.5 kW, SC power changes from 2 to 5 kW, and wind farm power from 5 to 5.5 kW at 1 sec in order to meet AC load demand. The AC load power demand is shown in Figure 9 which changes from 10 to 20 kW at 1 sec.

The 3-ph voltages and currents of the AC load are shown in Figure 10 which are observed to be sinusoidal with some harmonic content. The THD of the load voltage is determined using FFT analysis tool in 'powergui' calculated to be 5.29% shown in Figure 11. For case 1 operating condition the power balancing Table 2 at different instants of time is given. It shows the exchange of powers between the modules of the AC/DC micro grids.
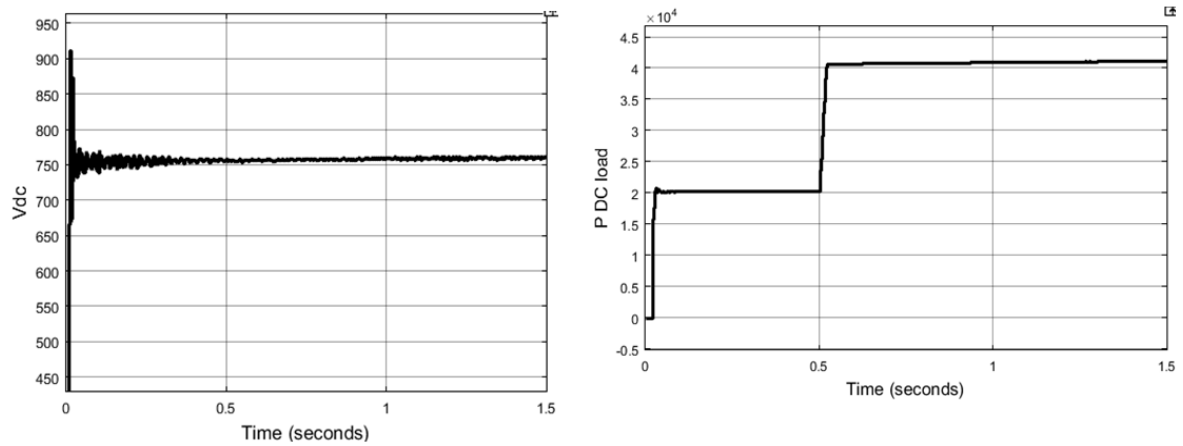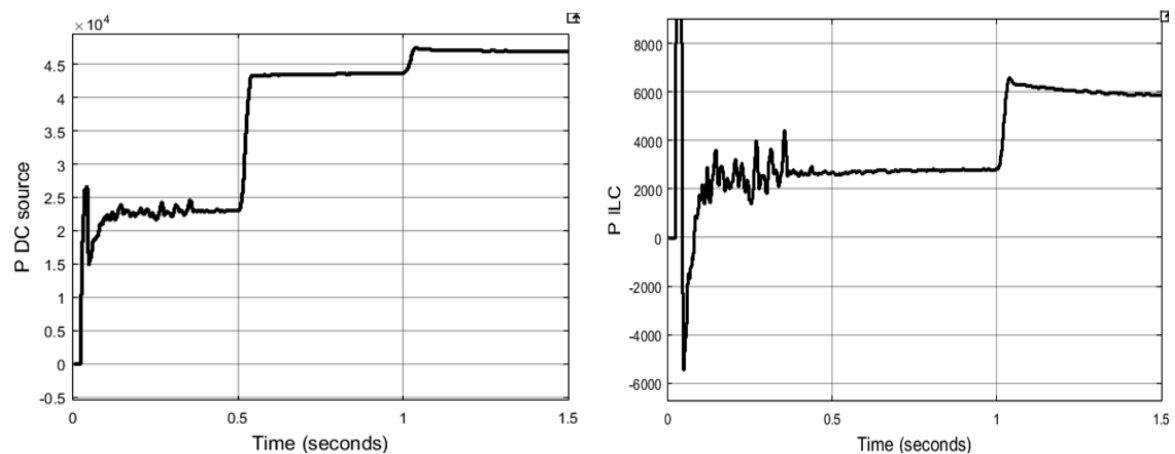

Figure 6. DC link voltage and load demand on the DC MG for case 1

Figure 7. Total power delivered by DC MG and injected power to AC MG through ILC for case 1
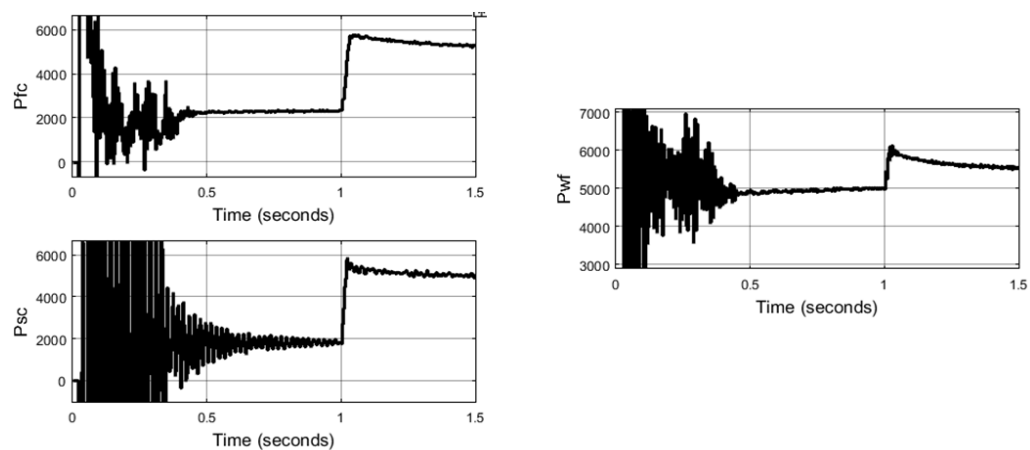
Figure 8. AC MG powers of Fuel cell plant, SC module, and wind farm for case 1
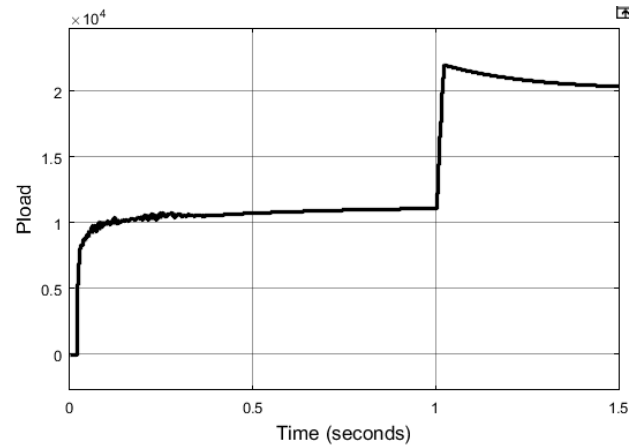
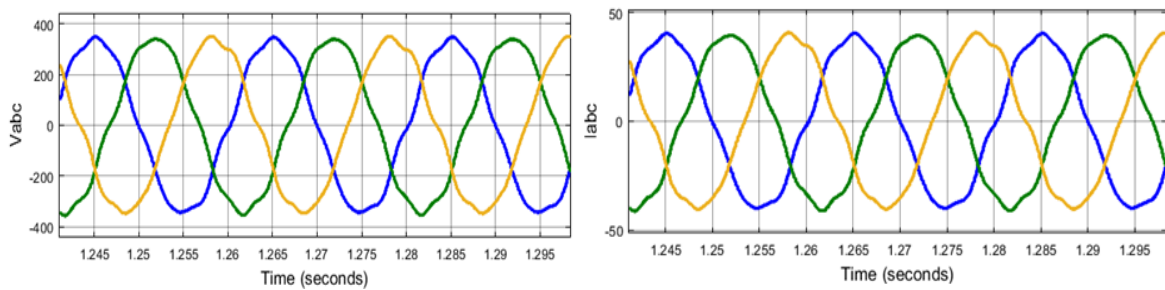Figure 9. AC load power for case 1

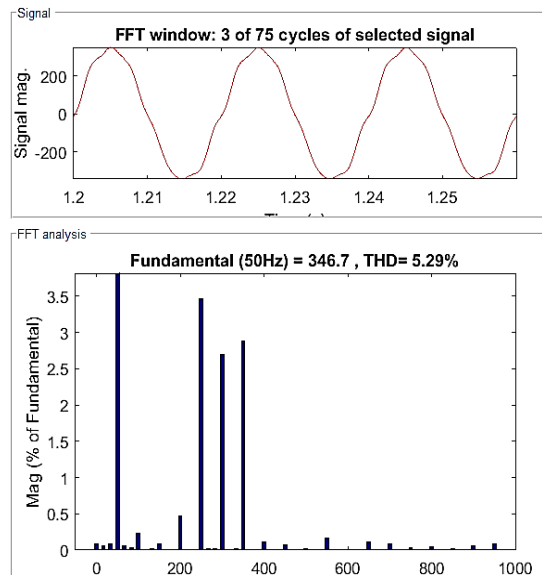Figure 10. 3-ph voltages and currents of AC load for case 1

Figure 11. THD of AC load voltage for case 1

As per Table 2, the power demand on the DC varies from 20kW to 40kW at 0.5 sec, and power demand on the AC side varies from 10 to 20 kW at 1 sec. The Ppv is always maintained at 22 kW as there is no change in solar irradiation. As per the change in load demand initially during low power demand the battery stores 20 kW of power and later it discharges up to 5 kW when the power demand increases. The wind farm power in the DC MG increases from 20 to 40 kW when the wind speed increases at 0.5 sec. The fuel cell and SC modules maintain the same powers of 2 kW during 0-1 sec which change to 5 kW at 1sec when the AC

load demand increases. In any given condition the DC link voltage is maintained near 750 V and the AC side single phase RMS voltage is maintained between 240 to 252 V. As per IEEE 519-2022 standard the THD of the voltage below 1 kV has to be maintained below 6%. As observed in Table 2 the THD of the PCC voltage is maintained near to 5% in any time range, considered to be below the standard value.

Table 2. Case 1 power balancing

Name of the parameter	0-0.5 sec	0.5-1 sec	1-1.5 sec
P_{pv}	22 kW	22 kW	22 kW
P_{bat}	-20 kW	2k W	5 kW
DC P_{wf}	20 kW	40 kW	40 kW
P_{ILC}	3 kW	3 kW	6 kW
P_{fc}	2 kW	2 kW	5.5 kW
P_{sc}	2 kW	2 kW	5 kW
AC P_{wf}	5 kW	5 kW	5.5 kW
$P_{dc\ load}$	20 kW	40 kW	40 kW
$P_{ac\ load}$	10 kW	10 kW	20 kW
DC link voltage	751 V	751 V	752 V
AC RMS voltage	247 V	252 V	242 V
THD of AC voltage	5.4%	5.41%	5.26%

4.2. Case 2: change in solar irradiation and wind speed

In this case the loads are maintained constant at 40 kW on DC MG and 20 kW on AC MG. The solar irradiation is varied from 1000 W/mt^2 to 300 W/mt^2 at 0.5 sec and wind speed is dropped to 8 mt/sec at 1 sec which was previously at 12 mt/sec. The voltage and power graphs of the modules for this case are recorded and plotted in Figure 12. As per the change in solar irradiation at 0.5 sec, Figure 12 shows the PV source power changes from 22 to 6 kW, wind power changes from 20 to 2 kW, battery power changes from 5 kW to 20-20 kW to 40 kW at 0.5 and 1sec respectively. In any given condition the DC link voltage is maintained at 750 V as shown in Figure 13 validating the stability of the system.

The DC load power also shown in Figure 13 is constant 40 kW throughout the simulation time. Figure 14 shows the total power delivered by the DC MG in case 2 recorded at 46 kW in any time interval. The power delivered by the ILC from DC MG to AC MG is 5.5 kW throughout the simulation also shown in Figure 14, as there is no change in load demand on either of the MG. The powers of the AC MG modules are shown in Figure 15 with fuel cell plant power at 5 kW, wind power at 5.5 kW, and SC power at 4.5 kW discharging. The AC load power measured is shown in Figure 16 with the value remaining constant at 20 kW throughout the simulation.

Figure 17 is the 3-ph voltage and current of AC load in case 2 operating condition. Even in this case 2 the voltage and current remain sinusoidal and the THD is maintained low. The THD of the load voltage for case 2 is shown in Figure 18 calculated to be 5.29%. The parametric comparison Table 3 has the power balancing values of the modules at different instants of time along with RMS and THD of the voltages.
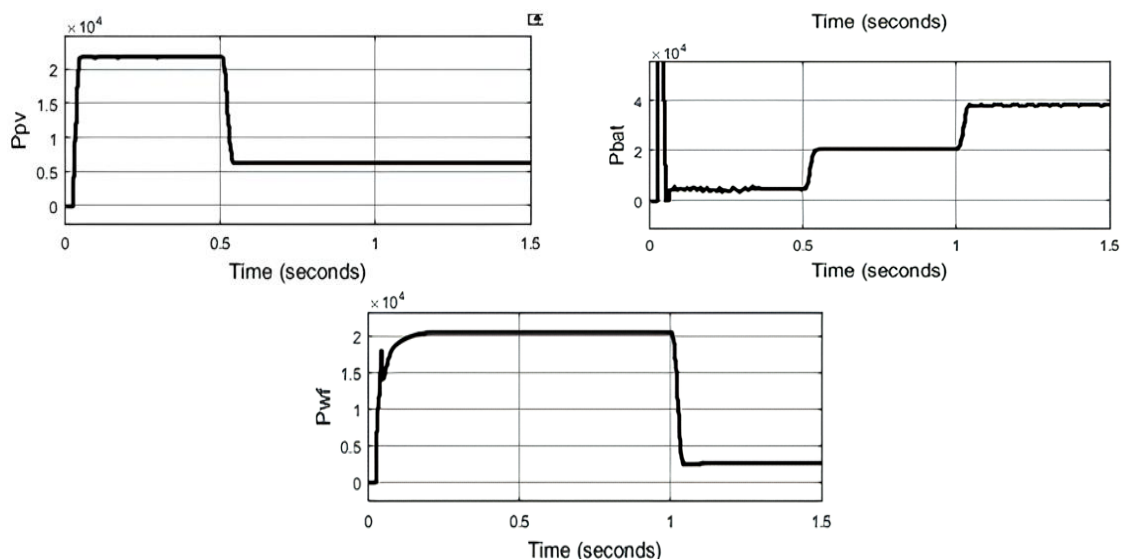

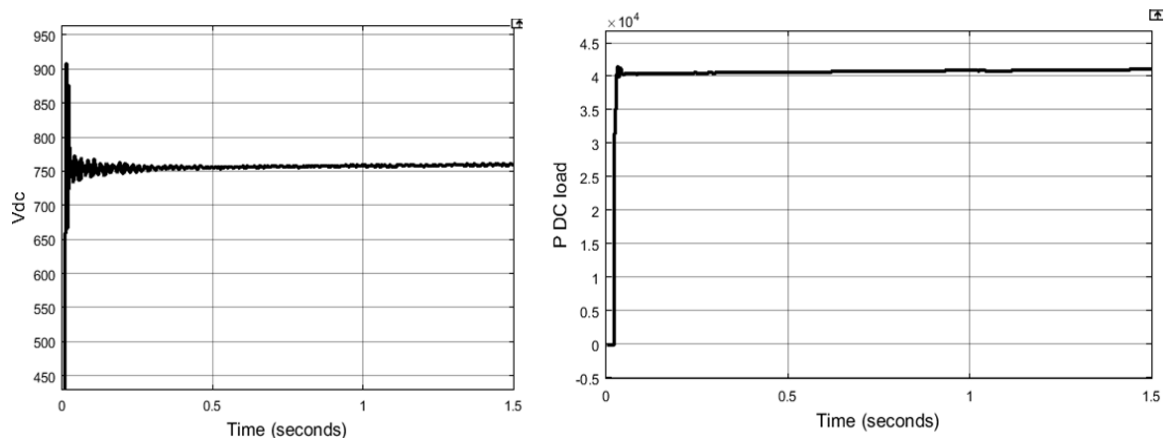Figure 12. DC MG power of PV source, battery module, and wind farm on DC MG for case 2

Figure 13. DC link voltage and load power on the DC MG for case 2
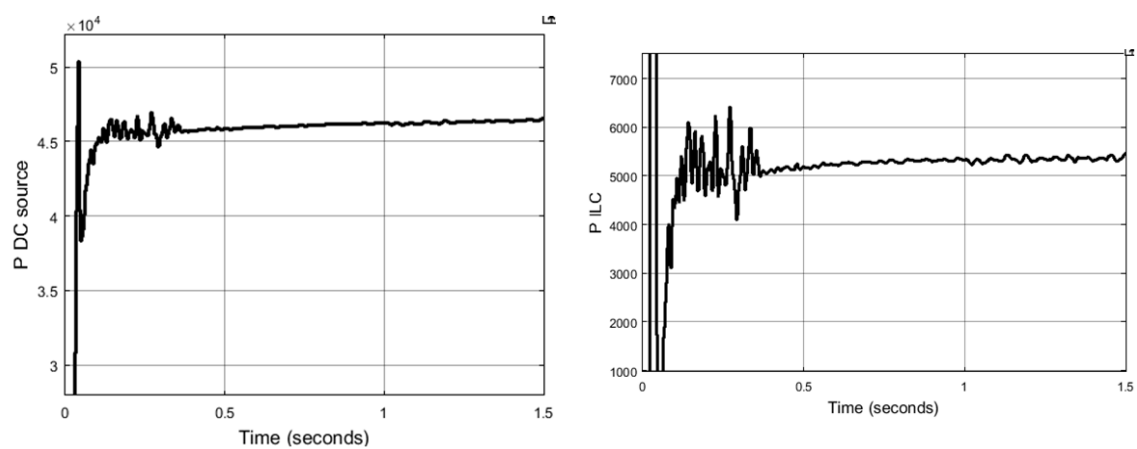

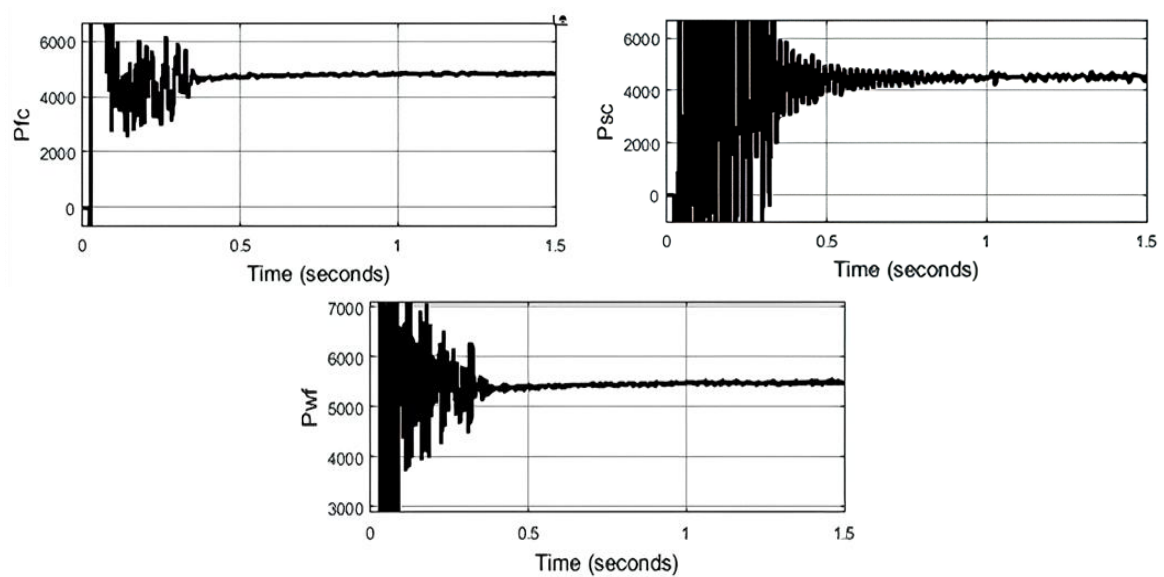Figure 14. Total power delivered by DC MG and power injected to AC MG for case 2

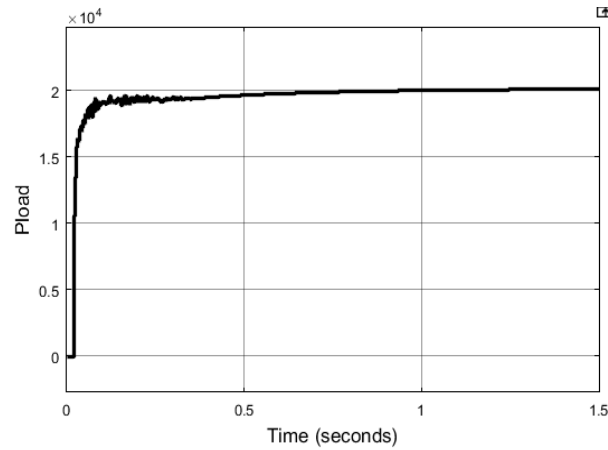Figure 15. AC MG powers of fuel cell plant, SC module, and wind farm for case
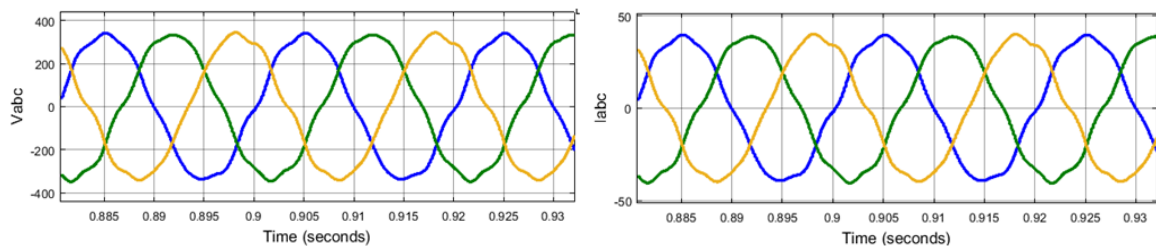
Figure 16. AC load power for case 2

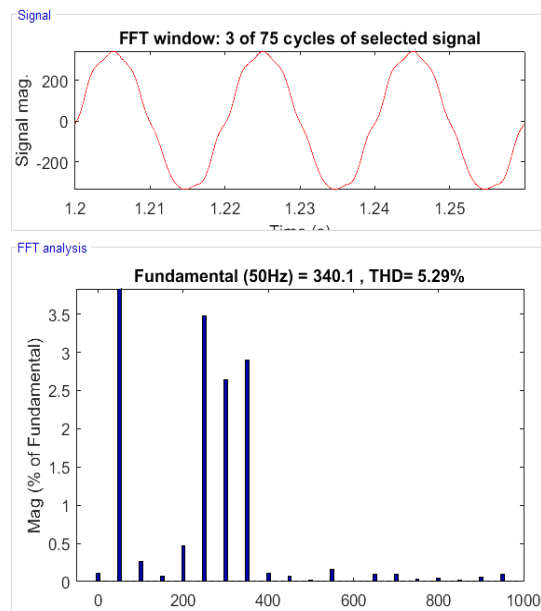Figure 17. 3-ph voltages and currents of AC load for case 2

Figure 18. THD of AC load voltage for case 2

In case 2 the DC load and the AC are maintained constant through the simulation at 40 kW and 10 kW respectively. Due to the change in solar irradiation at 0.5 sec the Ppv is dropped from 22 to 6 kW. Later on, when the wind speed is dropped at 1sec the wind power on the DC MG is dropped from 20 to 2 kW. In order to maintain the DC load power at 40kW the battery discharges to compensate the deficit renewable powers. The

battery power discharge increases from 5 to 20 kW and 20 to 40 kW at 0.5 sec and 1 sec respectively. The AC side MG modules fuel cell plant, SC module, and wind farm dispatch constant powers of 5 kW, 4.5 kW, and 5.5 kW. In this case, the DC link voltage is also maintained near 750 V, and the AC RMS voltage at 236 to 240 V. Even in this case, the THD of the PCC voltage is also maintained below 6% as per regulation.

Table 3. Case 2 power balancing

Name of the parameter	0-0.5 sec	0.5-1 sec	1-1.5 sec
P_{pv}	22 kW	6 kW	6 kW
P_{bat}	5 kW	20 kW	40 kW
DC P_{wf}	20 kW	20 kW	2 kW
P_{ILC}	5.5 kW	5.5 kW	5.5 kW
P_{fc}	5 kW	5 kW	5 kW
P_{sc}	4.5 kW	4.5 kW	4.5 kW
AC P_{wf}	5.5 kW	5.5 kW	5.5 kW
$P_{dc\ load}$	40 kW	40 kW	40 kW
$P_{ac\ load}$	10 kW	10 kW	10 kW
DC link voltage	750 V	752 V	751 V
AC RMS voltage	236 V	239 V	240 V
THD of AC voltage	5.32%	5.29%	5.27%

5.   CONCLUSION

As per the results generated by the simulation of the proposed hybrid MG system with multiple renewable and energy storage modules, it is determined that the loads on either of the MG are compensated in any given condition. The load compensation is achieved even during sudden change of load on DC or AC MG and even during natural resource variation. The voltages on the DC link and AC link are maintained stable for any given disturbances caused in the modules. The THD of the AC load voltage is maintained near to 5% at any condition occurred on the MG system. The ILC operates robustly with faster response rate delivering the required power to the load as per the demand. The ILC power delivery changes as per the load variation and environmental conditions, maintaining the voltage levels on AC MG or DC MG at reference set points. As per the power balancing tables, the DC and AC loads are compensated with full power during any operating condition validating the performance of the ILC. The stable DC and AC voltages also present the robustness of the ILC for the extreme conditions created on the hybrid MG.

REFERENCES

[1]   M. Jayachandran and G. Ravi, "Design and optimization of hybrid micro-grid system," *Energy Procedia*, vol. 117, pp. 95–103, Jun. 2017, doi: 10.1016/j.egypro.2017.05.111.
[2]   K. Zhang, M. Su, Z. Liu, H. Han, X. Zhang, and P. Wang, "A distributed coordination control for islanded hybrid AC/DC microgrid," *IEEE Systems Journal*, vol. 17, no. 2, pp. 1819–1830, Jun. 2023, doi: 10.1109/JSYST.2023.3242119.
[3]   K. C, S. M V, G. Singaram, U. K. A, M. K, and S. R, "Review of hybrid microgrid power management using renewable energy sources," in *2023 9th International Conference on Advanced Computing and Communication Systems (ICACCS)*, IEEE, Mar. 2023, pp. 1491–1496. doi: 10.1109/ICACCS57279.2023.10112787.
[4]   M. Biglarahmadi, A. Ketabi, H. R. Baghaee, and J. M. Guerrero, "Integrated nonlinear hierarchical control and management of hybrid AC/DC microgrids," *IEEE Systems Journal*, vol. 16, no. 1, pp. 902–913, Mar. 2022, doi: 10.1109/JSYST.2021.3050334.
[5]   E. E. Pompodakis, G. C. Kryonidis, C. Demoulias, and M. C. Alexiadis, "A generic power flow algorithm for unbalanced islanded hybrid AC/DC microgrids," *IEEE Transactions on Power Systems*, vol. 36, no. 2, pp. 1107–1120, Mar. 2021, doi: 10.1109/TPWRS.2020.3012815.
[6]   Z. Qu, Z. Shi, Y. Wang, A. Abu-Siada, Z. Chong, and H. Dong, "Energy management strategy of AC/DC hybrid microgrid based on solid-state transformer," *IEEE Access*, vol. 10, pp. 20633–20642, 2022, doi: 10.1109/ACCESS.2022.3149522.
[7]   J. Khodabakhsh and G. Moschopoulos, "Simplified hybrid AC–DC microgrid with a novel interlinking converter," *IEEE Transactions on Industry Applications*, vol. 56, no. 5, pp. 5023–5034, Sep. 2020, doi: 10.1109/TIA.2020.2996537.
[8]   H. Shi and K. Sun, "Bridge-to-bridge independent control method for dual-active-bridge interlinking converter," *IEEE Transactions on Power Electronics*, vol. 37, no. 8, pp. 8757–8761, Aug. 2022, doi: 10.1109/TPEL.2022.3150895.
[9]   S. P. Bihari *et al.*, "A comprehensive review of microgrid control mechanism and impact assessment for hybrid renewable energy integration," *IEEE Access*, vol. 9, pp. 88942–88958, 2021, doi: 10.1109/ACCESS.2021.3090266.
[10]   F. S. Al-Ismail, "DC microgrid planning, operation, and control: a comprehensive review," *IEEE Access*, vol. 9, pp. 36154–36172, 2021, doi: 10.1109/ACCESS.2021.3062840.
[11]   A. Rajkumar and S. Gangatharan, "A novel solar PV equipped flexible AC/DC microgrid based energy management for effective residential power distribution," *IEEE Canadian Journal of Electrical and Computer Engineering*, vol. 45, no. 3, pp. 328–338, 2022, doi: 10.1109/ICJECE.2022.3189687.
[12]   S. Gangatharan, M. Rengasamy, R. M. Elavarasan, N. Das, E. Hossain, and V. M. Sundaram, "A novel battery supported energy management system for the effective handling of feeble power in hybrid microgrid environment," *IEEE Access*, vol. 8, pp. 217391–217415, 2020, doi: 10.1109/ACCESS.2020.3039403.
[13]   L. A. Aloo, P. K. Kihato, S. I. Kamau, and R. S. Orenge, "Modeling and control of a photovoltaic-wind hybrid microgrid system using GA-ANFIS," *Heliyon*, vol. 9, no. 4, p. e14678, Apr. 2023, doi: 10.1016/j.heliyon.2023.e14678.

[14]　U. T. Salman, F. S. Al-Ismail, and M. Khalid, "Optimal sizing of battery energy storage for grid-connected and isolated wind-penetrated microgrid," *IEEE Access*, vol. 8, pp. 91129–91138, 2020, doi: 10.1109/ACCESS.2020.2992654.

[15]　P. S. Kumar, R. P. S. Chandrasena, V. Ramu, G. N. Srinivas, and K. V. S. M. Babu, "Energy management system for small scale hybrid wind solar battery based microgrid," *IEEE Access*, vol. 8, pp. 8336–8345, 2020, doi: 10.1109/ACCESS.2020.2964052.

[16]　S. Ghosh, S. Chattopadhyay, and S. Samanta, "A synchronous reference frame based decentralized control architecture for inverters connected to an autonomous microgrid," in *2019 IEEE Applied Power Electronics Conference and Exposition (APEC)*, IEEE, Mar. 2019, pp. 540–547. doi: 10.1109/APEC.2019.8721904.

[17]　A. Kumar, R. Garg, and P. Mahajan, "Modified synchronous reference frame control of solar photovoltaic-based microgrid for power quality improvement," *Arabian Journal for Science and Engineering*, vol. 46, no. 2, pp. 1001–1018, Feb. 2021, doi: 10.1007/s13369-020-04789-9.

[18]　A. N. Azmi, N. Salim, and A. Khamis, "Analysis of an energy storage sizing for grid-connected photovoltaic system," *Indonesian Journal of Electrical Engineering and Computer Science*, vol. 16, no. 1, pp. 17–24, Oct. 2019, doi: 10.11591/ijeecs.v16.i1.pp17-24.

[19]　A. Ordono, E. Unamuno, J. A. Barrena, and J. Paniagua, "Interlinking converters and their contribution to primary regulation: a review," *International Journal of Electrical Power & Energy Systems*, vol. 111, pp. 44–57, Oct. 2019, doi: 10.1016/j.ijepes.2019.03.057.

[20]　C. Wang, C. Deng, and G. Li, "Control strategy of interlinking converter in hybrid microgrid based on line impedance estimation," *Energies*, vol. 15, no. 5, p. 1664, Feb. 2022, doi: 10.3390/en15051664.

[21]　F. S. Adi, H. Song, and J.-S. Kim, "Interlink converter controller design based on system identification of DC sub-grid model in hybrid AC/DC microgrid," *IFAC-PapersOnLine*, vol. 52, no. 4, pp. 45–50, 2019, doi: 10.1016/j.ifacol.2019.08.153.

[22]　Z. Tang, Y. Yang, and F. Blaabjerg, "An interlinking converter for renewable energy integration into hybrid grids," *IEEE Transactions on Power Electronics*, vol. 36, no. 3, pp. 2499–2504, Mar. 2021, doi: 10.1109/TPEL.2020.3018585.

[23]　P. Rahimzadehkivi, G. Kadkhodaei, and M. Hamzeh, "Control and operation of the proposed interlinking converter in a DC-AC-DC hybrid microgrid based on the proposed modes of operation," in *2019 27th Iranian Conference on Electrical Engineering (ICEE)*, IEEE, Apr. 2019, pp. 819–824. doi: 10.1109/IranianCEE.2019.8786724.

[24]　J. Wang, C. Dong, C. Jin, P. Lin, and P. Wang, "Distributed uniform control for parallel bidirectional interlinking converters for resilient operation of hybrid AC/DC microgrid," *IEEE Transactions on Sustainable Energy*, vol. 13, no. 1, pp. 3–13, Jan. 2022, doi: 10.1109/TSTE.2021.3095085.

[25]　H. Zhang, M. Saeedifard, X. Wang, Y. Meng, and X. Wang, "System harmonic stability analysis of grid-tied interlinking converters operating under AC voltage control mode," *IEEE Transactions on Power Systems*, vol. 37, no. 5, pp. 4106–4109, Sep. 2022, doi: 10.1109/TPWRS.2022.3191132.

BIOGRAPHIES OF AUTHORS

Mamatha Seeramshetti ⓘ 🔍 SC 🔗 is a research scholar at Osmania University Hyderabad. She received her B.Tech. degree in Electrical & Electronics Engineering from JNTU, Hyderabad in 2006 & M.Tech. degree in Electrical Engineering from Shivaji University Kolhapur, Maharastra in 2010. She worked as assistant professor in Anurag University, Hyderabad from 2012 to 2022 and she worked as assistant professor in Aurora Engineering college, Hyderabad from 2011 to 2012. Her research interests include renewable energy systems, power electronic converters, microgrid systems, and power system applications. She can be contacted at email: mamata.seeramshetti@gmail.com.

Mallesham Gaddam ⓘ 🔍 SC 🔗 is a professor in the Electrical Engineering Department at Osmania University Hyderabad. He received his B.Tech., M.Tech., Ph.D., and post-doctoral in Electrical Engineering from Osmania University, IIT Delhi, and Yale University, in 2000, 2002, 2013, & 2016, respectively. His research interests are soft computing applications to design/control of microgrid/smart grid-based systems and power quality problems, renewable energy, power system control, optimization control, automation, and optimization. He can be contacted at email: drgm@osmania.ac.in.